

Determination Method of Buckling Load for Eccentric Cementing Casing Based on Adjacent Balance Criterion

Guijie Yu¹, Ruihe Wang², Weiguo Li³

China University of Petroleum (East China), Qingdao, Shandong, China

¹yuguijie@upc.edu.cn; ²wangrh@upc.edu.cn; ³liwg@upc.edu.cn

Abstract- Eccentric cementing status always occurs in the period of well completion in complex formation. Under this condition, buckling failure of casing has greater impact on normal production. According to adjacent balance criterion and higher differential equation, a determination method of buckling load for eccentric cementing casing was established. This avoids complex modeling and discretization processes when determining the critical buckling load of casing, and geometrical and physical parameters can directly be put in the formula of critical buckling load. There exists 8.3% relative error, comparing critical load from the formula with the result by using finite element method. That means the results are accurate. This method has the advantage of direct calculation and is easy for engineering applications without complex modeling and discretization processes.

Keywords- Eccentric Cementing; Casing; Adjacent Balance Criterion; Higher Differential Equation; Buckling; Critical Load; FEM

I. INTRODUCTION

Eccentric cementing means there appears eccentric annulus between the casing and borehole wall because the casing in the borehole is not centered. When cementing, the mud cannot be completely replaced by cement slurry. Part of cement sheath between wall and casing after the solidification of cement contacts with casing closely, and other part contacts with underground liquid. The state calls eccentric cementing status (Fig. 1), which often occurs in horizontal well section^[1]. It is the condition that does not meet the requirements of cementing. This condition often appears in well completion of complex formation^[2]. Obviously, eccentric cementing status lies in axis of casing. The casing and cement contact with formation closely. On the ring of casing, only partially external circular surfaces of casing and cement contact with formation. Partially external circular surfaces of casing contacts with cement and formation, other meets with no borehole, annular space is full of formation liquid and mud. The load on casing is the hydrostatic pressure, which is the load of partially external circular surfaces by underground liquid (Fig. 2). The entire cement circle on the outer surface of casing could improve the collapsing strength^[3]. The paper^{[4]~[8]} studied the collapsing strength in common condition. In this paper, according to adjacent balance criterion, casing deformation of eccentric cementing status was studied and the analysis method for collapsing strength of eccentric cementing casing was confirmed by means of mathematical analysis solution^[9]. And the example was shown.

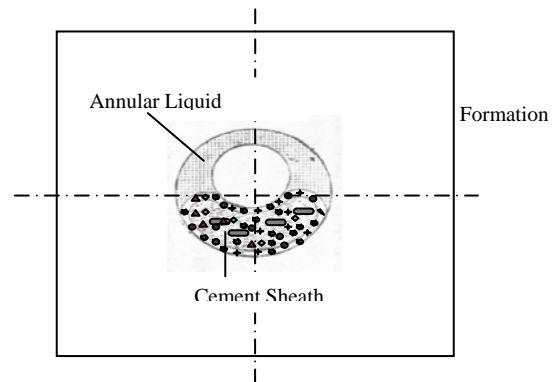


Fig. 1 Eccentric cementing chart

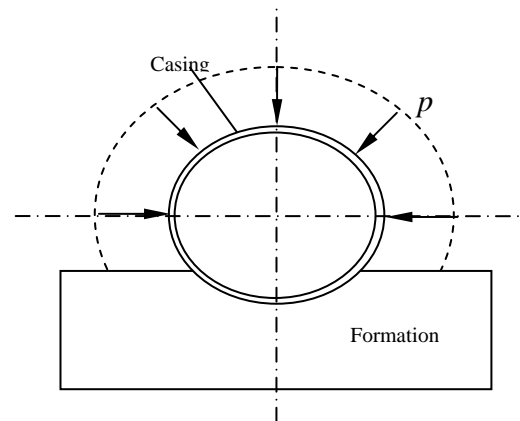


Fig. 2 Eccentric cementing mechanical model

II. SIMPLIFICATION OF MECHANICAL MODEL FOR ECCENTRIC CEMENTING STATUS CASING

Suppose there was considerable length for eccentric casing along axis (length of bare casing was beyond the range of constraint by cement), and it can be supposed as indefinite length. In order to simplify the issue, the physical dimensions of casing without cement were assumed: length as l along axis (considerable length), circumference size was expressed by centre angle of casing middle surface. That is $2\theta_0$. Because the size of bare casing along axis was big enough, there was no influence between constraint along axis and circle. When studying the buckling deformation of eccentric cementing status casing, take unit length of casing (ring) for study. The ring could be replaced by the circle in which average diameter of casing lay. Mechanical model was showed as Fig. 3.

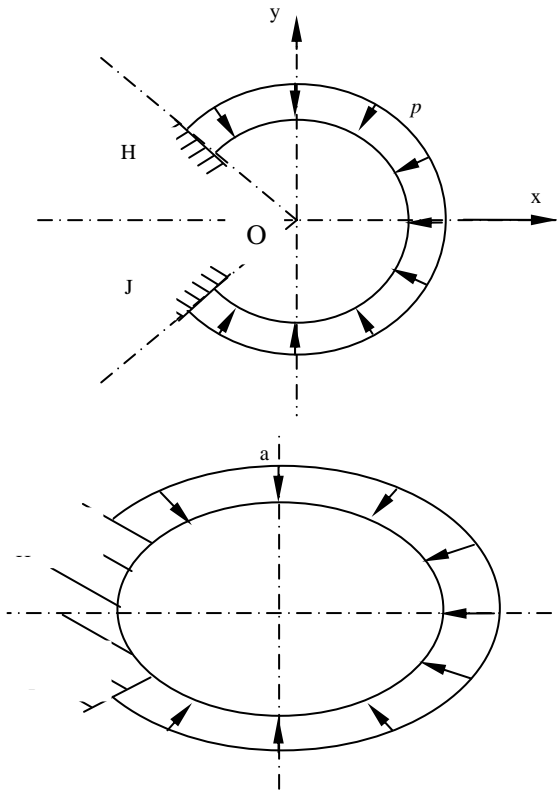


Fig. 3 Chart of mechanical model

III. RELATION BETWEEN THE DEFORMATION OF RING AND THE LOAD

As shown in Fig. 3b: unit length of the ring, average radius (the radius of middle surface) a , wall thickness t . Since $\frac{t}{a} \ll 1$, the casing was thin-walled. Dots (Fig. 4) were expressed with polar coordinates (r, θ) .

Without deformation at ring, the geometrical relationship was:

$$\begin{cases} x = r \cos \theta \\ y = r \sin \theta \\ z = r - a \\ (ds)^2 = (rd\theta)^2 \end{cases} \quad (1)$$

According to energy principle, under the load of hydrostatic pressure P , deformation appeared at the ring, and the equation between deformations of local fixed ring and load^[10] was:

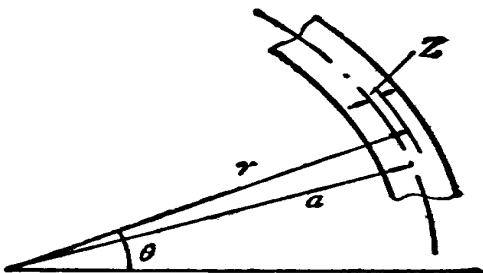


Fig. 4 Thin-walled dots

$$\begin{cases} [\frac{V'+W}{a} + \frac{1}{2}(\frac{V-W'}{a})^2]' + \frac{1}{Ea^2}(\frac{V-W'}{a})' \\ - [\frac{V'+W}{a} + \frac{1}{2}(\frac{V-W'}{a})^2](\frac{V-W'}{a}) \\ - \frac{pa}{EA_0}(\frac{V-W'}{a}) = 0 \\ \frac{I}{A_0a^2}(\frac{V-W'}{a})' - [\frac{V'+W}{a} + \frac{1}{2}(\frac{V-W'}{a})^2] \\ - a\{[\frac{V'+W}{a} + \frac{1}{2}(\frac{V-W'}{a})^2](\frac{V-W'}{a})\}' \\ - \frac{pa}{EA_0}(\frac{V'+W}{a}) = \frac{pa}{EA_0} \end{cases} \quad (2)$$

In which:

V, W —Displacement component of middle surface of the ring along circumferential and radial, m;

E —Modulus of elasticity of the ring, Pa;

A_0 —Sectional area of the ring, m²;

I —Moment of inertia of section relative to middle surface, m⁴.

IV. BUCKLING ANALYSIS OF THE RING

Under the axisymmetric load, for the entire load P , there were two types of shape for the stability of ring. One was circular stability balance; the other was noncircular stability balance. Obviously, from circular stability balance to noncircular stability balance, there must be a balance in the form of critical state, which the load was corresponding to was called critical load, written as p_{cr} .

Assume circumferential and radial displacement component of circular stability balance as (V_0, W_0) , and circumferential and radial displacement component of noncircular stability balance as $(V_0 + \Delta v, W_0 + \Delta w)$. Circular configuration and noncircular configuration both met Equation (2). In which $(\Delta v, \Delta w)$ was infinite small incremental. For configuration of circular stability balance, there was:

$$V_0 = V_0' = W_0' = 0 \quad (3)$$

Then, take (V, W) to configuration of noncircular stability balance, (V, W) could be showed as following.

$$\begin{cases} V = \Delta v \\ W = W_0 + \Delta w \end{cases} \quad (4)$$

Take Equation (3) and (4) to Equation (2), and $(\Delta v, \Delta w)$ was considered. Omit high order, we got:

$$\begin{cases} EA_0 a^2 [(\Delta v)' + (\Delta w)'] \\ + EI [(\Delta v) - (\Delta w)']'' \\ - EA_0 a W_0 [(\Delta v) - (\Delta w)'] \\ - p a^3 [(\Delta v) - (\Delta w)'] = 0 \\ EI [(\Delta v) - (\Delta w)']''' \\ - EA_0 a^2 [(\Delta v)' + (\Delta w)']'' \\ - EA_0 a W_0 [(\Delta v) - (\Delta w)'] \\ - p a^3 [(\Delta v) + (\Delta w)] = 0 \end{cases} \quad (5)$$

Due to symmetry:

$$W_0 = -\frac{p a^2}{EA_0} \quad (6)$$

Take Equation (6) to Equation (5), the stability equation of local fixed ring impacted by hydrostatic pressure was obtained.

$$\begin{cases} A_0 a^2 [(\Delta v)' + (\Delta w)'] + \\ I [(\Delta v) - (\Delta w)']'' = 0 \\ EA_0 a^2 [(\Delta v)' + (\Delta w)'] \\ - EI [(\Delta v) - (\Delta w)']''' \\ + p a^3 [(\Delta v) + (\Delta w)] = 0 \end{cases} \quad (7)$$

According to adjacent balance criterion^[10], $(\Delta v, \Delta w)$ in Equation (7) was circumferential and radial displacement increment of middle surface, which was from circular stability to noncircular stability of local fixed ring. Clearly, $(\Delta v, \Delta w)$ was the function of centre angle θ of ring. According to the feature of structure symmetry and load symmetry, and $(\Delta v, \Delta w)$ was the function of centre angle θ , the function was the general solution for Equation (7), and it must meet the following boundary conditions.

$$\begin{cases} \Delta v|_{-\theta_0} = (\Delta v)'|_{-\theta_0} = 0 \\ \Delta w|_{-\theta_0} = (\Delta w)'|_{-\theta_0} = 0 \\ (\Delta w)'|_{\theta=0} = 0 \end{cases} \quad (8)$$

Suppose : $a_1 = EA_0 a^2, a_2 = EI, a_3 = p a^3$

$$\begin{cases} X = (\Delta v)' + (\Delta w) \\ Y = (\Delta v) - (\Delta w)' \end{cases} \quad (9)$$

Equation (7) can be rewritten as:

$$\begin{cases} a_1 X' + a_2 Y'' = 0 \\ a_1 X - a_2 Y''' + a_3 [X - Y'] = 0 \end{cases} \quad (10)$$

To Equation (7) and (10), analytic solutions can be obtained with high differential equation method.

Assume:

$$Z = \begin{pmatrix} X \\ Y \\ Y' \\ Y'' \end{pmatrix} \quad (11)$$

Then:

$$Z' = \begin{pmatrix} X' \\ Y' \\ Y'' \\ Y''' \end{pmatrix} \quad (12)$$

Equation (10) can be rewritten as first-order equations.

$$\begin{pmatrix} X' \\ Y' \\ Y'' \\ Y''' \end{pmatrix} + \begin{pmatrix} 0 & 0 & 0 & \frac{a_2}{a_1} \\ 0 & 0 & -1 & 0 \\ 0 & 0 & 0 & -1 \\ -\frac{a_1 + a_3}{a_2} & 0 & \frac{a_3}{a_2} & 0 \end{pmatrix} \begin{pmatrix} X \\ Y \\ Y' \\ Y'' \end{pmatrix} = 0 \quad (13)$$

That was

$$Z' + AZ = 0 \quad (14)$$

In which A was

$$-A = \begin{pmatrix} 0 & 0 & 0 & -\frac{a_2}{a_1} \\ 0 & 0 & 1 & 0 \\ 0 & 0 & 0 & 1 \\ \frac{a_1 + a_3}{a_2} & 0 & -\frac{a_3}{a_2} & 0 \end{pmatrix} \quad (15)$$

Characteristic polynomial for Equation (14)

$$|\lambda I + A| = \lambda^2 \left(\lambda^2 + \frac{a_3}{a_2} + \frac{a_3}{a_1} + 1 \right) = 0 \quad (16)$$

Characteristic value for Equation (16):

$$\begin{cases} \lambda_1 = 0 \text{ (double root)} \\ \lambda_2 = \sqrt{\frac{a_3}{a_2} + \frac{a_3}{a_1} + 1} \cdot i \\ \lambda_3 = -\sqrt{\frac{a_3}{a_2} + \frac{a_3}{a_1} + 1} \cdot i = -\lambda_2 \end{cases} \quad (17)$$

So that three equations were acquired as following.

$$\begin{cases} (-A - \lambda_1 I)^2 u = 0 \\ (-A - \lambda_2 I) u = 0 \\ (-A - \lambda_3 I) u = 0 \end{cases} \quad (18)$$

Take $n_1 = 2, n_2 = 1, n_3 = 1$, and the basic solution for Equation (18) was:

$$\xi_1 = \alpha \begin{pmatrix} 1 \\ 0 \\ a_1 + a_3 \\ a_3 \\ 0 \end{pmatrix} + \beta \begin{pmatrix} 0 \\ 1 \\ 0 \\ 0 \end{pmatrix}, \xi_2 = \gamma \begin{pmatrix} \frac{a_2}{a_1} \lambda_2 \\ 1 \\ \lambda_2 \\ \lambda_2^2 \end{pmatrix}, \xi_3 = \tau \begin{pmatrix} \frac{a_2}{a_1} \lambda_3 \\ 1 \\ \lambda_3 \\ \lambda_3^2 \end{pmatrix} \quad (19)$$

Suppose $\eta = (\eta_1, \eta_2, \eta_3, \eta_4)^T = \xi_1 + \xi_2 + \xi_3$, the relationship among $\alpha, \beta, \gamma, \tau$ was

$$\begin{cases} \alpha = \eta_1 + \frac{a_2 a_3 \eta_3 - a_2 (a_1 + a_3) \eta_4}{a_1 a_2 + a_2 a_3 + a_3 a_1} \\ \beta = \eta_2 - \frac{\eta_4}{\lambda_2^2} \\ \gamma = \frac{\eta_4 (a_1 a_2 + a_2 a_3 + a_3 a_1) + a_1 a_3 \eta_3 \lambda_2 - a_1 (a_1 + a_3) \eta_1 \lambda_2}{2 \lambda_2^2 (a_1 a_2 + a_2 a_3 + a_3 a_1)} \\ \tau = \frac{\eta_4 (a_1 a_2 + a_2 a_3 + a_3 a_1) - a_1 a_3 \eta_3 \lambda_2 + a_1 (a_1 + a_3) \eta_1 \lambda_2}{2 \lambda_2^2 (a_1 a_2 + a_2 a_3 + a_3 a_1)} \end{cases}$$

Take $\alpha, \beta, \gamma, \tau$ to Equation (19), the expression of ξ_1, ξ_2, ξ_3 can be obtained.

The form of solution for Equation (14) was

$$\phi(t) = \sum_{j=1}^3 e^{\lambda_j t} \left[\sum_{i=0}^{n_j-1} \frac{(-A - \lambda_j I)^i}{i!} \right] \xi_j = [I - tA] \xi_1 + e^{\lambda_2 t} \xi_2 + e^{\lambda_3 t} \xi_3 \quad (20)$$

Assume $\eta = (1, 0, 0, 0)^T$. Take $(0, 1, 0, 0)^T, (0, 0, 1, 0)^T$ and $(0, 0, 0, 1)^T$ to $\phi(t)$, and four linearly independent solutions $\varphi_i(t)$ were got. Then from Equation (11)

$$Z = (X, Y, Y', Y'')^T = (\varphi_1(t), \varphi_2(t), \varphi_3(t), \varphi_4(t)) C \quad (21)$$

In which $C = (c_1, c_2, c_3, c_4)^T$, constant vector. So

$$\begin{cases} X = a_1 a_3 c_1 + [a_2 a_3 - a_2 a_3 \cos \mu t] c_3 + \frac{\mu a_2 \sin \mu t}{a_1} c_4 \\ Y = a_1 (a_1 + a_3) t c_1 + c_2 + \left[a_2 (a_1 + a_3) t + \frac{a_1 a_3}{\mu} \sin \mu t \right] c_3 + (1 + \cos \mu t) c_4 \end{cases} \quad (22)$$

In which

$$\mu = \sqrt{\frac{a_3}{a_2} + \frac{a_3}{a_1} + 1}$$

Equation (9) can be rewritten as

$$\begin{pmatrix} \Delta v' \\ \Delta w' \end{pmatrix} = \begin{pmatrix} 0 & -1 \\ 1 & 0 \end{pmatrix} \begin{pmatrix} \Delta v \\ \Delta w \end{pmatrix} + \begin{pmatrix} X \\ -Y \end{pmatrix} \quad (23)$$

Equation (23) was nonhomogeneous linear system of differential equations. The proper vector corresponding to the proper value ($\bar{\lambda}_1 = i, \bar{\lambda}_2 = -i$) of coefficient matrix

$$\bar{A} = \begin{pmatrix} 0 & -1 \\ 1 & 0 \end{pmatrix} \text{ met the following equation.}$$

$$(\bar{\lambda} I - \bar{A}) \bar{\xi} = 0 \quad (24)$$

That is:

$$\begin{pmatrix} \bar{\lambda} & 1 \\ -1 & \bar{\lambda} \end{pmatrix} \begin{pmatrix} \bar{\xi}_1 \\ \bar{\xi}_2 \end{pmatrix} = 0 \quad (25)$$

$$\begin{cases} \bar{\lambda} \bar{\xi}_1 + \bar{\xi}_2 = 0 \\ -\bar{\xi}_1 + \bar{\lambda} \bar{\xi}_2 = 0 \end{cases} \quad (26)$$

Solution vector corresponding to it was

$$\begin{cases} \bar{\xi}_1 = i \\ \bar{\xi}_2 = 1 \end{cases} \quad (27)$$

and

$$\begin{cases} \bar{\xi}_1 = -i \\ \bar{\xi}_2 = 1 \end{cases} \quad (28)$$

So $\tau_1 = (i, 1)^T, \tau_2 = (-i, 1)^T$, and basic solutions for Equation (23) were

$$\bar{\Phi}(\theta) = \begin{pmatrix} i e^{i\theta} & -i e^{-i\theta} \\ e^{i\theta} & e^{-i\theta} \end{pmatrix} \quad (29)$$

Inverse of Equation (29) was

$$\bar{\Phi}^{-1}(\theta) = \begin{pmatrix} -\frac{i}{2} e^{-i\theta} & \frac{1}{2} e^{-i\theta} \\ \frac{i}{2} e^{i\theta} & \frac{1}{2} e^{i\theta} \end{pmatrix} \quad (30)$$

The form of general solution for nonhomogeneous linear system of differential equations (Equation (23)) was

$$\begin{pmatrix} \Delta v \\ \Delta w \end{pmatrix} = \bar{\Phi}(\theta) \bar{\Phi}^{-1}(-\theta_0) \eta + \bar{\Phi}(\theta) \int_{-\theta_0}^{\theta} \bar{\Phi}^{-1}(s) \begin{pmatrix} X(s) \\ -Y(s) \end{pmatrix} ds \quad (31)$$

What can be obtained according to the first and second term of Equation (8) was

$$\begin{pmatrix} \Delta v \\ \Delta w \end{pmatrix} = \int_{-\theta_0}^{\theta} \begin{pmatrix} \cos(\theta-s) & -\sin(\theta-s) \\ \sin(\theta-s) & \cos(\theta-s) \end{pmatrix} \begin{pmatrix} X(s) \\ -Y(s) \end{pmatrix} ds \quad (32)$$

$$0 = \begin{pmatrix} \Delta v \\ \Delta w \end{pmatrix} \Big|_{\theta=-\theta_0} = \begin{pmatrix} 1 & 0 \\ 0 & 1 \end{pmatrix} \begin{pmatrix} X(-\theta_0) \\ -Y(-\theta_0) \end{pmatrix} \quad (33)$$

So

$$\begin{cases} 0 = a_1 a_3 c_1 + (a_2 a_3 - a_2 a_3 \cos \mu \theta) c_3 - \frac{a_2 \mu}{a} \sin \mu \theta c_4 \\ 0 = a_1 (a_1 + a_3) \theta c_1 - c_2 + \left[a_2 (a_1 + a_3) \theta + \frac{a_1 a_3}{\mu} \sin \mu \theta \right] c_3 - (1 + \cos \mu \theta) c_4 \end{cases} \quad (34)$$

From Equation (32)

$$\Delta w = \int_{-\theta_0}^{\theta} [X(s) \sin(\theta-s) - Y(s) \cos(\theta-s)] ds$$

The expression for function $X(s)$ and $Y(s)$ can be seen in Equation (22).

What can be obtained according to the first and second term of Equation (8) was

$$\begin{aligned} 0 = \Delta v \Big|_{\theta_0} &= [-a^2 \sin \theta + a(a_1 + a_3) \theta \cos \theta] c_1 + (1 - \cos \theta) c_2 \\ &+ [-a a_2 \sin \theta + a_2 (a_1 + a_3) \theta \cos \theta + \left(\frac{a a_3}{\mu} - a_2 a_3 \right) \frac{\sin(\mu+1)\theta}{2(\mu+1)} - \left(a_2 a_3 + \frac{a a_3}{\mu} \right) \frac{\sin(\mu-1)\theta}{2(\mu-1)}] c_3 \\ &+ \left[(1 - \cos \theta) + \left(\frac{1}{2} \frac{\mu_2}{2 a_1} \right) \frac{1 - \cos(\mu+1)\theta}{(\mu+1)} - \left(\frac{1}{2} + \frac{\mu_2}{2 a_1} \right) \frac{1 - \cos(\mu-1)\theta}{(\mu-1)} \right] c_4 \end{aligned} \quad (35)$$

Third-order equations consist of four constant coefficients c_1, c_2, c_3, c_4 :

$$\begin{cases} 0 = a_1 a_3 c_1 + (a_2 a_3 - a_2 a_3 \cos \mu \theta) c_3 - \frac{a_2 \mu}{a} \sin \mu \theta c_4 \\ 0 = a_1 (a_1 + a_3) \theta c_1 - c_2 + \left[a_2 (a_1 + a_3) \theta + \frac{a_1 a_3}{\mu} \sin \mu \theta \right] c_3 - (1 + \cos \mu \theta) c_4 \\ 0 = [-a^2 \sin \theta + a(a_1 + a_3) \theta \cos \theta] c_1 + (1 - \cos \theta) c_2 \\ + [-a a_2 \sin \theta + a_2 (a_1 + a_3) \theta \cos \theta + \left(\frac{a a_3}{\mu} - a_2 a_3 \right) \frac{\sin(\mu+1)\theta}{2(\mu+1)} - \left(a_2 a_3 + \frac{a a_3}{\mu} \right) \frac{\sin(\mu-1)\theta}{2(\mu-1)}] c_3 \\ + \left[(1 - \cos \theta) + \left(\frac{1}{2} \frac{\mu_2}{2 a_1} \right) \frac{1 - \cos(\mu+1)\theta}{(\mu+1)} - \left(\frac{1}{2} + \frac{\mu_2}{2 a_1} \right) \frac{1 - \cos(\mu-1)\theta}{(\mu-1)} \right] c_4 \end{cases} \quad (36)$$

Or be written as

$$\begin{aligned} A_{11} c_1 + A_{12} c_2 + A_{13} c_3 + A_{14} c_4 &= 0 \\ A_{21} c_1 + A_{22} c_2 + A_{23} c_3 + A_{24} c_4 &= 0 \\ A_{31} c_1 + A_{32} c_2 + A_{33} c_3 + A_{34} c_4 &= 0 \end{aligned} \quad (37)$$

In which

$$\begin{cases} A_{11} = a_1 a_3, A_{12} = 0, A_{13} = a_2 a_3 - a_2 a_3 \cos \mu \theta, A_{14} = -\frac{a_2 \mu}{a} \sin \mu \theta \\ A_{21} = a_1 (a_1 + a_3) \theta, A_{22} = -1, A_{23} = a_2 (a_1 + a_3) \theta + \frac{a_1 a_3}{\mu} \sin \mu \theta, A_{24} = -(1 + \cos \mu \theta) \\ A_{31} = -a^2 \sin \theta + a(a_1 + a_3) \theta \cos \theta, A_{32} = 1 - \cos \theta, \\ A_{33} = -a a_2 \sin \theta + a_2 (a_1 + a_3) \theta \cos \theta + \left(\frac{a a_3}{\mu} - a_2 a_3 \right) \frac{\sin(\mu+1)\theta}{2(\mu+1)} - \left(a_2 a_3 + \frac{a a_3}{\mu} \right) \frac{\sin(\mu-1)\theta}{2(\mu-1)} \\ A_{34} = (1 - \cos \theta) + \left(\frac{1}{2} \frac{\mu_2}{2 a_1} \right) \frac{1 - \cos(\mu+1)\theta}{(\mu+1)} - \left(\frac{1}{2} + \frac{\mu_2}{2 a_1} \right) \frac{1 - \cos(\mu-1)\theta}{(\mu-1)} \end{cases}$$

What was obtained was the proportional relationship among the four coefficients. Firstly, make $c_4 = 1$, so c_1 and c_3 were acquired from the first and third equation. Then take them to

the second equation, we got c_2 . The expression of $\begin{pmatrix} \Delta v \\ \Delta w \end{pmatrix}$

was acquired by taking them to Equation (32).

On the basis of analysis, Δv and Δw were the function of E, A_0, a, I, P and θ , it meant they were the function of a_1, a_2, a_3 and θ in analyzing. Under the axial symmetry load, to make the ring be in critical state from circular stability balance to noncircular stability balance, there must have the following equations for all θ .

$$\begin{cases} \Delta v = 0 \\ \Delta w = 0 \end{cases} \quad (38)$$

Meanwhile, critical load p_{cr} of buckling failure of ring was gained.

V. EXAMPLES

Finite element model of eccentric cementing status was showed in Fig. 5.

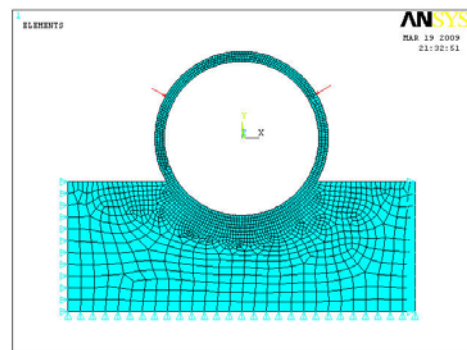


Fig. 5 Element analysis model of structure

Basic parameter of casing: grade of steel was N80; external diameter (D) was 139.7 and wall thickness was 7.72; modulus of elasticity was 216GPa; poisson's ratio was 0.25. Stratum parameter: modulus of elasticity was 216GPa;

Poisson's ratio was 0.3. angle of bare pipe θ_0 equaled to 120° symmetrically. The load was external pressure P .

Take the basic parameters above to the coefficients of Equation (7) and (9), we got:

$$a = 69.85 \times 10^{-3} (\text{m}); \quad A_0 = 7.72 \times 10^{-6} (\text{m}^2);$$

$$I = 3.8342 \times 10^{-11} (\text{m}^4); \quad a_1 = EA_0 a^2 = 7909.8713 (\text{Nm}^2);$$

$$a_2 = EI = 0.8052 (\text{Nm}^2); \quad a_3 = 0.06985 p (\text{N/m}^2).$$

After taking a_1, a_2, a_3 and θ_0 to Equation (36), when given P an initial value p_0 , the first maximal value p_{cr} of P was 155.1 MPa through trial.

Under the condition above, the hydrostatic pressure p_{cr} was 155.1 MPa when theoretical eccentric cementing appeared stability disruption.

Finite element method:

According to the physical model established with the parameter above, take plane182 for discretization to the structure. Make horizontal displacement of left and right side limited, as well as vertical displacement of underside. Casing would be affected by external pressure p .

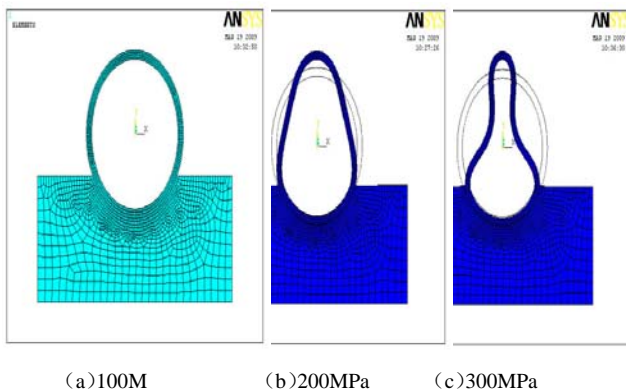


Fig. 6 Deflection of eccentric cementing casing

There existed no relative displacement between casing and layer. Finite element model could be seen in Fig. 5. There were 1780 elements and 2008 nodes in total.

In Fig. 6a to 6c, structural deforming graphs were showed under the condition of external pressure 100MPa, 200MPa and 300MPa. It can be seen from the graphs that both Fig. 6b and Fig. 6c were in unstable state. The relationship between radial displacement and external pressure on the peak of casing was given by Fig. 7, from which the break of displacement appeared when external pressure was 168MPa. That was to say, critical pressure was 168Mpa when it was unstable.

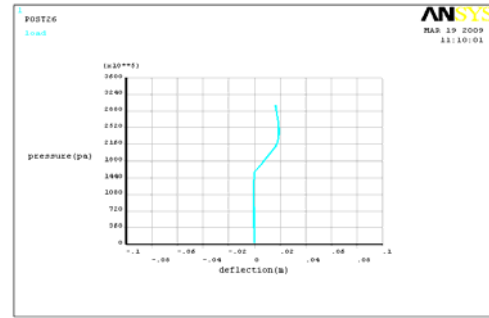


Fig. 7 Radial displacement vs. pressure of casing at acme

Compare finite element results with theoretical results, error of calculation was: $\frac{168 - 155.1}{155.1} = 8.3\%$. Theoretical results were close to finite element results. And the accuracy of theoretical analysis was validated.

VI. CONCLUSION

The method, buckling analysis of eccentric cementing status casing, is an easy and valid way for the study of collapse resistance. It is not as complex as the physical finite element modeling process, but the stable load can be acquired by directly entering the relevant parameters. For the convenience of calculation, accuracy and convenience for engineering applications, it is easy for theory to be applied to engineering project.

REFERENCES

- [1] Xu Huifeng. Drilling Technical Manual (3) (Cement) [M]. Petroleum industry Press, Beijing: 1990. 7.
- [2] Wu Jiang, Hao Junfang. Permit eccentricity of well cementation casing [J]. Petroleum Drilling Techniques, 1989, 17(4): 42-47.
- [3] Song Ming, Influencing Tendencies of Cement Sheath on Casing Retaining Capacity [J], Oil Drilling & Production Technology, 2002, 24(4):7-9.
- [4] Cui xiaobing, Zhang Hong, Li Zihou, An Wenhua, Song Zhi. Research on Reasonable Free Segment Length of Deep Oil Well Casing String [J], Acta Petrolei Sinica, 1997, 18(1): 91-95.
- [5] Zhang Zhiquan, Wu Jiazhong, Luo Yue. Analysis and Countermeasures of Casing Deformation Causes in Gangxi Oil field [J], Journal of Jiangnan Petroleum Institute, 2002, 24(4): 83-84.
- [6] Fang Jun. Analysis of Loading Propekty of Casing and Cement Sheath Under Nonuniform Geologic Stress [J], Journal of the University of Petroleum, 1995,19(6):52-57.
- [7] Gao Xueshi, Fang Jun. Calculation Method for Collapse of Oil Casing Restrained by Concrete [J]. Journal of the University of Petroleum, 1994, 18(3):39-46.
- [8] Ma Xu, Lab Test of Destruction of Cement Sheath Outside Casing, China Petroleum Machinery, 2000, 28(4):15-18.
- [9] Li Weiguo, Tong Dengke. Numerical Computing Methods [M]. University of Petroleum Press, Shandong: 262-291(2008.10).
- [10] Chen Tiejun, Shen Huizhong. The Bucking of Structure [M]. Shanghai Science and Technology Literature Press, Shanghai: 111-120(1993, 12).

Two Dimensional Dynamic Modeling of Hydrodesulphurization Reactor

Peyman Mahinsa^{1,2}, Mohammad Taghi Sadeghi², Hamid Ganji^{1*}, Saeed Shokri¹

¹Process Development Division, Research Institute of Petroleum Industry, Tehran, IRAN

²Faculty of Chemical Engineering, Iran University of Science and Technology, Tehran, IRAN

ganjih@ripi.ir

Abstract- In this research a pseudo-homogeneous two-dimensional model was proposed to describe the dynamic behavior of a fixed-bed pilot-plant hydrodesulphurization reactor. The catalyst pellet used in this reactor was Co-Mo/Al₂O₃. At first, using the experimental data, a power law kinetic model was developed for hydrodesulphurization reaction. Then a pseudo-homogeneous two-dimensional dynamic model was proposed to describe the concentration profile in the reactor bed. The simulation obtained with the proposed dynamic model showed good agreement with experimental data and the sulfur concentration error in the reactor outlet was 3.8 percent compared to the experimental data. Two dimension modeling revealed that the radial variation of sulfur concentration is more in the reactor inlet than the outlet, but in general the concentration profile can be considered in one dimension. Unsteady reactor modeling showed that the transition time was higher in the reactor outlet and estimated to be 11667 seconds.

Keywords- Hydrotreating reactor, Dynamic Modeling, Two Dimension

I. INTRODUCTION

Hydrodesulphurization (HDS) is an important process in oil industry. The HDS process is essential to obtain fuels with improved quality and low polluting compounds and it is usually conducted in a fixed-bed catalytic reactor either in single gas-phase flow or two phases (gas and liquid) [1-3] and usually a trickle-flow regime may occur. In the trickle flow regime, the liquid reactant flows downward through the reactor in the form of thin laminar film droplets around the solid catalyst [4-6]. Modeling and simulation are commonly applied in the design, performance analysis, optimization, and scale-up of HDS reactors. More papers in modeling and simulation are in steady state but reliable three-phase reactor modeling and simulation should be based on dynamic heterogeneous models, which can be used not only for scale-up, start-up and operability studies, but also to obtain a meaningful continuity path to the steady state of the reactor, since dynamic models provide a realistic description of the transient states of three-phase reactors [7, 8]. The study of the dynamic behavior of the three phase reactor also helps designing the best control system in order to obtain a safe, efficient and profitable operation. Although the dynamic models are more complicated to formulate and to solve, they should be preferred over steady-state models because the numerical solution strategy of dynamic models is more robust than the solution of steady-state models [9-12].

Numerous papers have been published on steady state modeling of hydrotreating reactors. However, studies on dynamic modeling of such reactors are reported less in the open literature among which the two dimensional models are rarely reported. Julcour et. al.[13] investigated the dynamic of the three phase up-flow fixed bed reactor using a non-isothermal heterogeneous model. They compared a simplified

model with an extended one and concluded that the diffusion of hydrocarbons is not limiting agent so that the simplified model predicts accurately the reactor transient behavior. Hastaoglu and Jibril[12] modeled the transient gas-solid reactions in a fixed-bed reactor and applied to HDS reaction with the Langmuir-Hinshelwood mechanism. They validated the model through a comparison of experimental data from naphtha HDS pilot plant. Mederos et. al[14] investigated a dynamic heterogeneous one-dimensional model of trickle-bed hydrotreating reactor. They considered the hydrodesulphurization, hydrodenitrogenation and hydrodearomatization reactions and axial changes in concentration, partial pressure and temperature profiles were obtained with time. Chen and Ring[15] considered a pseudo homogeneous two dimensional reactor model of a fixed-bed hydrotreater and studied concentration and temperature profiles. Their model considered the heat conduction in the thermowell to predict the temperature difference between the thermowell and the catalytic bed. They concluded that if this difference is too high and ignored, could cause errors in the interpretation of pilot plant data. Mederos and Ancheyta [2] developed a dynamic heterogeneous one-dimensional model to predict the behavior of trickle-bed hydrotreating reactor with co-current and counter-current operation. They concluded that counter-current mode can have great potential to be used for deep hydrodesulfurization of oil fractions since it minimizes the inhibiting effect of some products in reactor zones where these species tend to concentrate in concurrent operation.

This paper reports experimental work and simulation results on the steady-state and dynamic behavior of a fixed-bed pilot-plant HDS reactor.

II. EXPERIMENTAL SECTION

The experiments were done in an isothermal pilot-plant reactor. The schematic diagram of the pilot plant setup is shown in fig. 1.

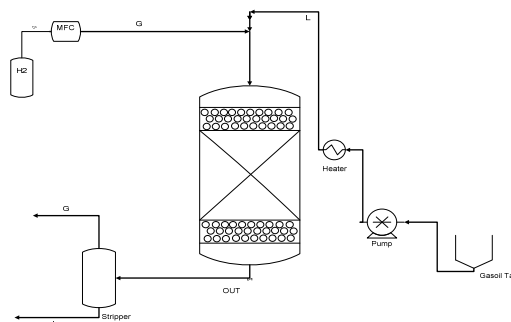


Fig 1. Schematic diagram of the pilot plant setup

The unit has been operated at temperature range of 340-380 °C and pressure range of 48-60 bar. Feed volumetric flow rate was 60-260 $\frac{cm^3}{h}$. The reactor length and internal diameter were 200 and 1.9 cm respectively and the catalytic bed length was 35 cm which was filled with CoMo/AL₂O₃ catalyst. Above and below catalyst bed were packed with glass beads to provide a uniform gas and liquid flow. Hydrodesulfurization unit needs two different kinds of feeds. One for activation that consists of Dimethyl disulfide, hydrogen sulfide and carbon disulfide and other is used for separation of sulfur.

III. MATHEMATICAL MODEL

The reactor which has been used in pilot plant was operated isothermally. In this research we considered a pseudo-homogeneous two-dimensional model with axial convective and radial dispersion of mass. The dynamic mass balance equation in the catalyst bed is

$$\epsilon_1 \frac{\partial C_i^l}{\partial t} = -U_1 \frac{\partial C_i^l}{\partial z} + \epsilon_1 D_a^l \frac{\partial^2 C_i^l}{\partial z^2} + \epsilon_1 D_r^l \left(\frac{\partial^2 C_i^l}{\partial r^2} + \frac{1}{r} \frac{\partial C_i^l}{\partial r} \right) - \rho_B \eta_j^l r_j^l \quad (1)$$

Where i=S, N, A

For catalyst pellets:

$$\frac{D_{ei}^l}{r_p^2} \frac{\partial}{\partial r_p} \left(r_p^2 \frac{\partial C_{f,i}^s}{\partial r_p} \right) + r_j^l \rho_s \quad (2)$$

Where i=S, H₂S, H₂

Using Eq. 2, the effectiveness factor can be calculated with the following equation:

$$\eta_j^l = \frac{3 \int_0^{R_p} r_j^l (C_s - T_s) r_p^2 dr_p}{r_j^l (C_{sli}^s - T_s^s)} \quad (3)$$

It was assumed that all holes of catalyst pellet were filled with liquid.

A. Model initial and boundary conditions and solution

For steady state and dynamic modeling it is necessary to define initial and boundary conditions. The initial and boundary conditions for liquid and solid phases are summarized in tables 1 and 2 respectively.

TABLE 1 INITIAL CONDITIONS

Condition	Liquid phase	Solid phase
z=0 0 ≤ r ≤ R	C _i ^l = (C _i ^l) ₀	
0 < z < L _B 0 ≤ r ≤ R		
z=L _B 0 ≤ r ≤ R		

TABLE 2 BOUNDARY CONDITIONS

condition	Liquid phase	Solid phase
z=0 0 ≤ r ≤ R		
z=L _B 0 ≤ r ≤ R		-
r=0 0 < z < L _B		-
r=R 0 < z < L _B		-

The numerical method chosen to solve the developed partial differential equations is orthogonal collocation method,

a type of weight residual method (WRM) for elliptic PDE with two spatial domains. The orthogonal collocation is applied on both domains to yield a set of algebraic equations [16-18].

IV. RESULTS

A. Kinetics Evaluation

The following power law rate equations were considered for sulfur conversion although other expressions are available:

$$r_{HDS} = k C_S^n \quad (4)$$

$$k = k_0 \exp \left(\frac{-E}{RT} \right) \quad (5)$$

In which three kinetics parameters (k₀, E, n) were unknown and to calculate them two basic assumptions were considered:

1. Isothermal reactor
2. Plug flow regime

Equation 4 can be written as:

$$\frac{1}{n-1} \left(\frac{1}{C_p^{n-1}} - \frac{1}{C_f^{n-1}} \right) = \frac{k}{LHSV} \quad (6)$$

Where C_f and C_p are sulfur concentration at reactor inlet and outlet respectively.

Kinetics parameters were obtained using Eq. 6 and fitting experimental data where the following kinetics equation was obtained with linear regression of 98.7 percent:

$$r_{HDS} = 64402.1 \exp \left(\frac{-92.66}{RT} \right) C_S^{1.4} \quad (7)$$

B. Steady State Results

The reactor governing equations have to be solved simultaneously to obtain sulfur axial concentration profile. Fig. 2 shows how sulfur concentration decreases in the liquid phase through the reactor.

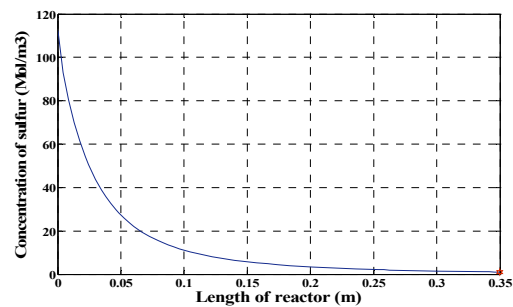


Fig 2. Sulfur axial concentration profile in liquid phase (feed rate: 140 cc/hr , P=50 bars inlet temperature=632.15 K)

The results reveal that there exists good agreement with experimental data and the sulfur concentration error in the reactor outlet was 3.8 percent compared to the experimental data and conversion was 99 percent. The partial pressure of H₂S in gas phase increases smoothly along the reactor bed as shown in Fig 3. But the H₂S concentration at the liquid phase increases and then decreases (Fig. 4). This phenomenon can be interpreted by mass transfer resistances. When the H₂S concentration in the liquid phase increases, the driving force of mass transfer from liquid to gas phase increases accordingly. This decreases the H₂S concentration in liquid phase.

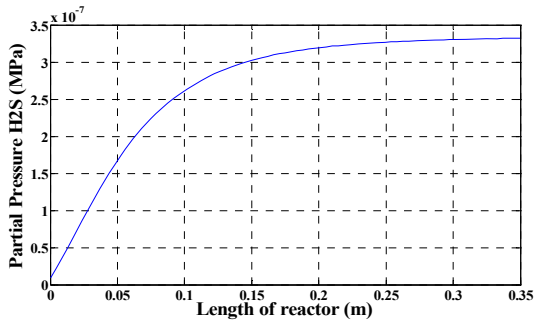


Fig 3. Partial pressure of H₂S in gas phase

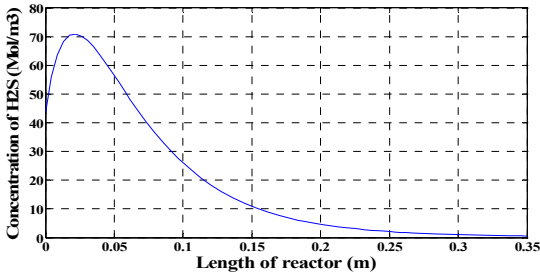


Fig 4. H₂S concentration profile in liquid phase

Radial sulfur concentration profiles were obtained at various axial sections of the reactor (Fig.5). Note that the radial variation of sulfur concentration decrease when approach the end of reactor.

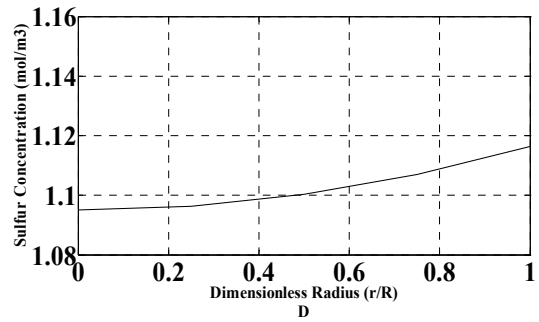
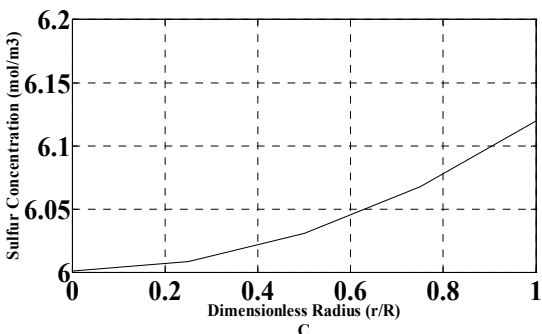
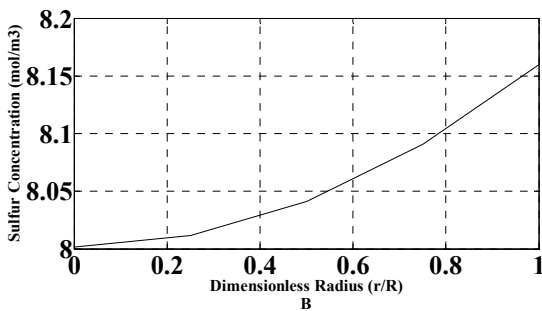
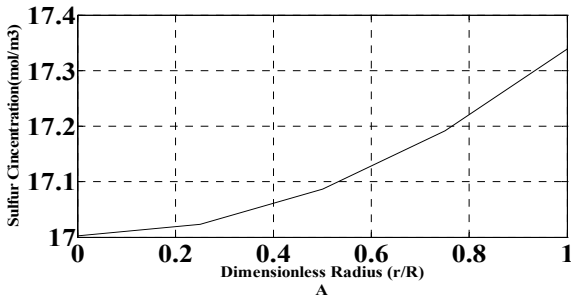


Fig 5. Sulfur radial concentration profile in liquid phase at various bed sections (feed rate: 140 cc/hr, P=50 bars, inlet temperature=632.15 K, A=0.25 Z, B=0.5 Z, C=0.75 Z, D=Z)

C. Dynamic Simulation

Figure 6 shows the variation of sulfur concentration at initial part of the catalytic bed (8.75 cm) and also at the reactor outlet with time. It was observed that the transition time was higher in the reactor outlet and estimated to be 11667 seconds

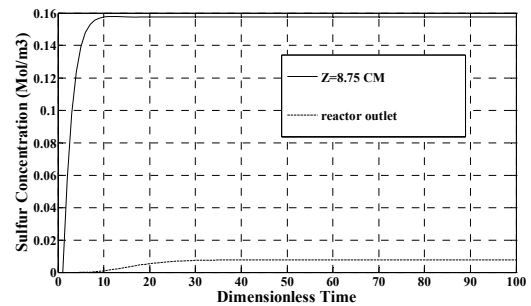


Fig 6. Sulfur concentration at 8.75 cm and the reactor outlet as a function of time (Feed rate: 140 cc/hr, P=50 bars inlet temperature=632.15 K, Dimension time is $\frac{U_1 t}{L \epsilon_1}$, $\epsilon_1 = 0.08$)

V. CONCLUSIONS

A mathematical reactor model has been developed to numerically simulate the steady-state and dynamic behavior of a pilot-plant hydrotreater. The pilot plant reactor has been operated isothermally. Simulation results revealed suitable agreement with the pilot-plant experimental data. Simulation results indicated that the axial sulfur concentration decreases in the liquid phase while the hydrogen sulfide partial pressure increases smoothly in the gas phase. Hydrogen sulfide concentration in the liquid phase increases first and then decreases. The reason of this behavior can be interpreted by mass transfer driving force from liquid to gas phase which increases when the H₂S Concentration in liquid phase increases. Two dimension modeling result indicated that there is not much radial concentration variation and one dimensional approach can be considered. Dynamic simulation results proved that the transition time to steady state increases when reach to the reactor outlet.

Nomenclature

- = Molar concentration of component i in the liquid phase, $C_i^L \left(\frac{Mol_i}{m^3}\right)$
- $C_{i,i}^s$ = Molar concentration of component i inside the solid filled with liquid phase, $\left(\frac{Mol_i}{m^3}\right)$
- d_p = Catalyst particle diameter, m

$D_{e,i}^L$ = Effective diffusivity of component i inside a porous catalyst, ($\frac{m^2}{s}$)

D_a^L = Mass axial dispersion coefficient of liquid phase, ($\frac{m^2}{s}$)

D_r^L = Mass radial dispersion coefficient of liquid phase, ($\frac{m^2}{s}$)

K_{app} = Apparent reaction rate constant

LHSV= Liquid hourly space velocity, (hr^{-1})

n = Reaction Order

P = Reactor Pressure, (MPa)

r = Radial reactor coordinate, (m)

r_p = Radius of particle, (m)

r_j^L =Rate of reaction j per unit of catalyst mass in the liquid phase, $\frac{Mol}{Kg_s.S}$

t = Time, s

t' = Dimensionless Time

z = Axial reactor coordinate, m

Greek Letters

ϵ_B = Catalyst bed void fraction or catalyst bed porosity

ϵ_S = Catalyst particle porosity

ρ_B = Catalyst bulk (or bed) density, $\frac{Kg}{m^3}$

ρ_f = Density at process conditions of f phase, $\frac{Kg}{m^3}$

η_j^L = Catalyst effectiveness factor of reaction j in the liquid phase

Subscripts

App = Apparent

B = Referred to reactor catalytic bed

f = Phase (gas, liquid or solid)

H_2 = Molecular hydrogen

H_2S = Hydrogen sulfide

L = Liquid phase

S = solid phase, inside catalyst pellet

REFERENCES

- [1] Vishwakarma, S. K.(2007) Sonochemical and Impregnated Co-W/ γ -Al O Catalysts:Performances and Kinetic Studies on Hydrotreatment of Light Gas Oil.
- [2] Mederos, F.S., Ancheyta, J. (2007) Mathematical modeling and simulation of hydrotreating reactors: Cocurrent versus countercurrent operations Applied Catalysis A: General 332 (1) ,8–21.
- [3] Ramachandran, P. A., Chaudhari, R. V. Three pPhase Catalytic Reactors; Gordon and Breach Science Publishers Inc.: London, 1983.
- [4] Doraiswamy, L.K., Sharma, M.M. (1984) Heterogeneous Reactions: Analysis, Examples, and Reactor Design; John Wiley & Sons: New York, 1984; Vol. 2, 374 pp.
- [5] Bhaskar, M., Valavarasu, G. (2002) Meenakshisundaram, A., Balaraman, K. S. Application of a Three Phase Heterogeneous Model to Analyse the Performance of a Pilot Plant Trickle Bed Reactor. Pet. Sci. Technol., 20 (3&4): 251–268.
- [6] Froment, G.F., Depauw, G.A., Vanrysselberghe, V. (1994) Kinetic Modeling and Reactor Simulation in Hydrodesulfurization of Oil Fractions. Ind. Eng. Chem. Res., 33 (12): 2975–2988.
- [7] Fabián S. Mederosa Ignacio Elizalde, Jorge Ancheyta, Steady-State and Dynamic Reactor models for Hydrotreatment of Oil Fractions: A Review, México, 2009.
- [8] Tarhan, M.O. (1983) Catalytic Reactor Design. McGraw-Hill: New York; 372 pp.
- [9] Chen, J., Ring, Z., Dabros, T. (2001) Modeling and Simulation of a Fixed-Bed Pilot-Plant Hydrotreater. Ind. Eng. Chem. Res., 40 (15): 3294–3300.
- [10] Wa'rna°, J., Salmi, T. (1996) Dynamic Modelling of Catalytic Three Phase Reactors. Comput. Chem. Eng., 20 (1): 39–47.
- [11] Salmi, T., Wa'rna°, J., Toppinen, S., Ro'nnholm, M., Mikkola, J.P. (2000) Dynamic Modelling of Catalytic Three-Phase Reactors for Hydrogenation and Oxidation Processes. Braz. J. Chem. Eng., 17 (4–7): 1023–1035.
- [12] Hastaoglu, M.A., Jibril, B.E. (2003) Transient Modeling of Hydrodesulfurization in a Fixed- Bed Reactor. Chem. Eng. Comm., 190 (2): 151–170.
- [13] Julcour C., Chaudhari R. V., Lelann J M., Wilhelm A. M., Delmas H. , Dynamic modeling of three phase upflow fixed-bed reactor including pore diffusion, Chem. Eng. And Proc., 41(2002)311-320.
- [14] Mederos F. S., Rodriguez J., Ancheyta J., and Arce E., Dynamic modeling and simulation of catalytic hydrotreating reactor, Energy & Fuels, 20(2006)936-945.
- [15] Chen, J., Ring, Z., Dabros, T. (2001) Modeling and Simulation of a Fixed-Bed Pilot-Plant Hydrotreater. Ind. Eng. Chem. Res., 40 (15): 3294–3300.
- [16] Villadsen, J., Michelsen, M.L., (1978) Solutions of Differential Equations Models by Polynomial Approximation. Prentice-Hall, Inc., New Jersey.
- [17] Hilfebrand, F., (1965) Method of Applied Mathematics, second ed., Prentice-Hall, Inc., New Jersey.
- [18] Mickley, H.S., Sherwood, T.K., Reed, C.E. (1990) Applied Mathematics in Chemical Engineering, second ed., McGraw-Hill, Delhi.

Ecotoxicity Assessment of Weathered Waste Oil in a Mexican Wetland

R. Uribe-Hernández*, M. A. Montes de Oca-García, M. A. Amezcua-Allieri, J. A. Zermeño- Eguía Lis, V. E. Martínez-Martínez

Safety and Environment Department, Mexican Petroleum Institute
Eje Central L. Cárdenas No. 152, Col. San Bartolo Atepehuacan, C.P. 07730, Mexico

*e-mail: ruribe@imp.mx

Abstract- The present study applied the ecotoxicity assessment through of a battery of bioassays used to determine toxicity potential in a tropical wetland impacted for oil waste industry. The bioassays applied were Microtox®, *Eisenia foetida*, *Glycine max* and *Triticum aestivum*. The total petroleum hydrocarbons (TPH) in soil was varied to 200,000 mg kg⁻¹. The PAHs between compounds detected was the benzo(a)pyrene (B(a)P). The results of bioassays showed a higher potential toxicity obtained in the zone 2 and 4 respect to control zone ($p < 0.001$). The results from the MANOVA analysis, determined the zone 2 with the bigger ecotoxicity potential regarding to others zones. The results showed a gradient of sensitivity soil toxicity as follows: Microtox® > *Eisenia foetida* > *Glycine max* > *Triticum aestivum* ($p < 0.05$). In case of both values, LC50 and EC 50 for (B(a)P) the best relationship ($r \approx 0.9$, $P < 0.05$) was obtained with phytoassays with *G. max* and *T. aestivum*.

Keywords- Ecotoxicity; TPH; PAH; B(a)P; Oil Waste; Bioassays; Wetland; Phytoassays; Tropical Wetland

I. INTRODUCTION

Wetlands are critically important wildlife habitats, often serving as breeding grounds for a wide variety of animal life. Wetlands recharge groundwater supplies and moderate stream flow by providing water to streams. Wetland vegetation and microorganisms also use excess nutrients for growth that can otherwise pollute surface water, such as nitrogen and phosphorus from fertilizers (US EPA, 2006).

Pollution, especially near urban areas or industrial, remains a serious threat to ecosystems. Fortunately, some countries have enacted special laws to protect wetlands, but much diligence is needed to that these protective measures are actively enforced. Since there is an absence of regulatory framework in Mexico to set toxicity test in order to promote environmental protection, remediation or ecological restoration, we used a set of bioassays to assess Mexican wetland which has been impacted by weathered waste oil.

Bioassays provide important information for the assessment of pollutant effects of chemicals or environmental samples. In contrast to chemical analyses, they also detect effects of multiple contaminants and metabolites (Eisentraeger et al., 2005). The use of a set of tests on species at different levels of biological organization and of biological approaches to complement physico-chemical analyses has been recommended for a refined evaluation of environmental risk.

Terrestrial plant and invertebrate (earthworm, collembola) tests have been selected on the basis of their ability to measure chemical toxicity to ecologically relevant test species during chronic assays which include at least one reproductive component among the measured endpoints (Eom et al., 2007).

Between pollutants of concern, we can identify total petroleum hydrocarbons (TPH), including polycyclic aromatic hydrocarbons (PAH). These compounds are residues from combustion, coke production, petroleum refining, and other high-temperature industrial processes (Bispo et al., 1999).

II. MATERIALS AND METHODS

A. Methods for Soil Sampling

Soil samples contaminated with hydrocarbons were taken from a tropical wetland (total area = 72 km²) located in the east central part of Mexico, between 17°10' and 22°38' N and between 93°55' and 98°38' W. Samples were taken from the top 50 cm soil layer (US EPA, 1998), as hydrophobic compounds are usually adsorbed (Riser-Roberts, 1998). Due to the presence of petroleum industry, the study area received irregular and uncontrolled disposal of waste oil for more than 5 decades. The study area was divided in four contaminated zones (Z) and one zone considered as control zone (Figure 1), according to previous studies that reported different levels of contamination (Uribe-Hernández et al, 2004), having the control zone the lowest levels of total petroleum hydrocarbons (TPH) and none of the 16 EPA priority polycyclic aromatic hydrocarbons (PAH). A total of 30 samples were taken per zone. The results show the mean value of triplicate samples.

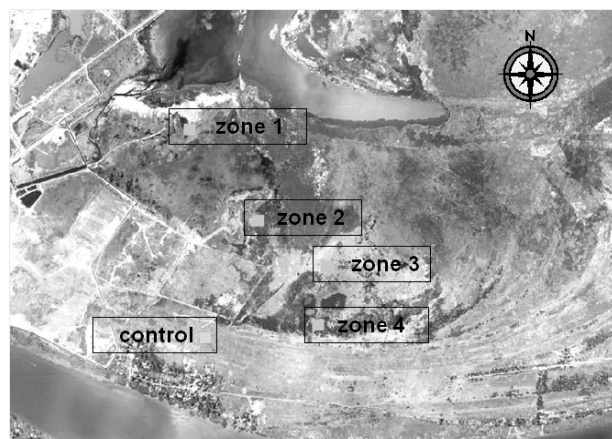


Figure 1 Wetland in Veracruz, Mexico. The aerial photo, scale: 1:5,000, shows the four zones of the study area. Between 17°10' and 22°38' North and between 93°55' and 98°38' West. 17°10' and 22°38' North

B. Methods For Hydrocarbon Analyses

Soil extract was obtained as follows: 50 g of soil was placed into an Erlenmeyer flask in addition to 1 g of anhydrous sodium sulphate (Sigma Aldrich®, Houston, TX, USA) and 50 ml dichloromethane (Merck, Bedford, MA, USA), stirring for 30 min, leaving it to rest for approximately

45 min, and filtering through fiberglass (Coatings Inc., Buffalo, NY, USA) to obtain the pure extract, finally covering hermetically to avoid evaporation of the solvent.

1) Total Petroleum Hydrocarbons:

Duplicate samples (40 g wet wt) of oily soils from each treatment were taken on each zone for determinations of TPH. Methylene chloride solvent was used in the Soxhlet extraction. The solvent extract was treated with silica gel to remove polar compounds and analysed by an infrared (IR) analyser (Perkin-Elmer) according to EPA Method 418.1 as TPH-IR. The calibration standard used in the TPH-IR method was 25% (v/v) n-hexadecane, 37.5% (v/v) isooctane, and 37.5% (v/v) chlorobenzene; absorption was measured in the IR spectral range of 3400–3500 cm⁻¹ (USEPA, 1979). TPH analysis was performed using the EPA 418.1 method, with a detection limit (dry base) of 68.8 mg kg⁻¹. This method was used only for hydrocarbon contamination screening.

2) Polycyclic Aromatic Hydrocarbons:

Polycyclic compounds (two-, three-, and four-, and five-ring PAH) were extracted using sonication and methylene chloride from 2 g of soil according to EPA Method 3550 and analysed by a direct injection GC/MS determination based on EPA Method 8270 (USEPA, 1988). The detection limit for each hydrocarbon is listed in Table 1.

TABLE I AVERAGE TPH AND PAH MEASURED IN THE SOIL OF THE WETLAND

Zone	TPH (mg kg ⁻¹)	PAH (mg kg ⁻¹)				B(a)P
		Phenanthrene	Anthracene	Fluorene	Benzo(a) Anthracene	
Z1	10,904 ±1,312	6.32 ±1.02	1.51 ±0.11	DL ^c	4.1 ±0.24	1.22 ±0.12
Z2	780,000 ±63,000	37.71 ±9.38	<DL ^b	9.03 ±1.23	DL ^d	2.03 ±0.22
Z3	298,000 ±28,022	<DL ^a	3.92 ±0.98	DL ^c	DL ^d	1.29 ±0.23
Z4	19,117 ±1,107	2.63 ±0.23	1.08 ±0.97	DL ^c	DL ^d	2.89 ±0.11
Control	105 ± 11	<DL ^a	<DL ^b	DL ^c	DL ^d	DL ^e

DL= Detection limit (mg kg⁻¹) ^a0.002, ^b0.007, ^c0.065, ^d0.067, ^e0.06.

C. Bioassays

To determine toxicity potential, bioassays were carried out at two levels of response; the first instance consisted of calculating the lethal toxicity (LC₅₀). In the second approach, we determined the sublethal toxic effects to obtain the effective concentration (EC₅₀ and EC₁), with the latter used to determine clean up levels.

The bioassays for toxicity were selected taking into account the ecologic niche for biologic group. *Glycine max* in addition to *Triticum aestivum* as plants in phytoassay analysis, *Eisenia foetida* as a mesofauna representative species, and Microtox[®] as microbiological bioassay. All tests were carried out in triplicate and results are the mean value.

Germination tests are important for soil evaluation because the toxic effects are observed by the inhibition or promotion of the seed and root, and, at later times, the growth process. For germination, certified seeds provided by the Productora Nacional de Semilla [National Producer of Seeds], Mexico, were used. Test conditions followed the guidelines of OECD (1984) and ISO (2003b) for *T. aestivum* and *G. max* in triplicate. Test temperature was kept at 22 ± 1 °C, exposure

time was 5 days, and the test volume was 15 ml (Petri dish diameter, 40 mm), using a light cycle of 16 h light/8 h dark (light 9000 lx). When 65% of the seeds from the negative test were germinated, the number of germinated seeds in each TPH extracts dilutions (0, 3.125, 6.25, 12.5, 25, 50, and 100%), were counted if their root was > 5 mm. 2-chloroacetamide (35 mg/l) was used as a positive control and distilled water as a negative control. The germination test was maintained within an environmental test chamber at a controlled temperature (23/15 °C day/night) and a 16:8 h (light: dark) photoperiod. A total of 10 seeds were exposed per dish. Dose-response curves were obtained to determine the lethal concentration 50 (LC₅₀) of the toxicant at different concentrations.

The phytotoxicity test to evaluate *Triticum aestivum* and *Glycine max* length was performed as follows. After the germination test, we transplanted each plant into agrolita (10 g) containing the TPH extracts (0, 3.125, 6.25, 12.5, 25, 50, and 100% from soil extract). The 16:8 h light: dark photoperiod was maintained, using cultivation lamps Philips SON/T Plus (400 W). All replicates were randomized for the position that they occupied. Testing time lasted 21 and 14 days for *Glycine max* and *Triticum aestivum*, respectively, to leave enough time for the first foliar primordia growth (US EPA, 1996). After the TPH exposure period had ended, biomass, in addition to the stem and root length, was measured in triplicate. The half maximal effective concentration (EC₅₀) was calculated for TPH, and the dose-response curve was obtained. In order to calculate the effective concentration (EC₁ and EC₅₀) for B(a)P for both *G. max* and *T. aestivum*, a dose-response curve was calculated using the dilutions mentioned above.

For the acute toxicity test (96 h) using *E. foetida*, organisms were acclimated before the bioassay took place. The lab conditions were established according to the ISO 11268 method (ISO, 2003a). The test was performed using the dilution extracts at 0, 3.125, 6.25, 12.5, 25, 50, and 100% with three replicates for each treatment. Placing Whatman cellulose paper disks No. 1 inside a Petri dish (9-cm diameter), 1 ml of the soil extract was distributed homogeneously on the paper, evaporating the solvent during 10 min. Then, 1 ml distilled water and 0.5 ml dimethyl sulfoxide at 1% were added as a vehicle for the assimilation of the toxicant. For the positive (+) and negative (-) tests, 1 ml dichloromethane and distilled water were added, respectively. A total of 10 organisms were exposed per dish. Dose-response curves were obtained to determine the lethal concentration 50 (LC₅₀) of the toxicant at different concentrations.

Microtox[®] was the method used for the bacterial toxicity evaluation. The bioluminescence reduction on *Vibrio fischeri* was measured with a photomultiplier coupled to a light sensor and toxicity results are expressed as EC₅₀ at a given time (Anzur, 1998). Soil toxicity was determined by analyzing elutriates from the contaminated soils, which were obtained with 1 g soil in 5 ml of a 35% NaCl solution, and making an extraction (at 25°C) by ultrasound (Cole-Parmer mod 8845-40, Vernon Hills, IL, USA) for 15 min (EPA 3552C method) (US EPA, 2000). The sample was filtered using membrane filters of 45-µm pore, and toxicity was analyzed during 5 and 15 min, by measuring the light emitted by bacteria, in comparison with a negative control. Toxicity was expressed as "Toxic Units, TU", where TU = 100/EC₅₀.

D. Statistical Analysis

Probit regression analysis was used to fit and determine the dose-response curve to calculate the lethal concentration

50 (LC₅₀) and effective concentrations 1 and 50 (EC₁ and EC₅₀, respectively). For each bioassay, one-way ANOVA was calculated to determine if there were statistically significant differences in the observed responses among the four zones and the control zone and to analyze if the answer was related to the degree of contamination in each area. MANOVA were performed for all the bioassays and their endpoints, together with the hydrocarbon chemical analyses, performing multiple post hoc tests by Tukey Honestly Significant Difference test. All statistical analyses were performed using the software SPSS® V.10.

III. RESULTS AND DISCUSSION

The results of the TPH and PAH levels are shown on Table 1. The highest level of TPH was found in Z2, followed by Z3; and Z1 and Z4 were relatively similar with the lowest levels. Although the control sample was not completely free of hydrocarbons, it had the lowest TPH level (105 mg kg⁻¹) and it had none of the 16 priority PAH. The rest of the priority PAH, not included on Table 1, were not detected in any of the zones or the control one.

In an average of 622 soil samples, TPH fractions contained 21.75 ± 16.12% saturated hydrocarbons, 32 ± 23% aromatic hydrocarbons, and 46.25 ± 28.28% asphaltenes. From the 16 EPA priority PAH analyzed, benzo(a)pyrene (B(a)P) exceeded the maximum permissible limit (2 mg kg⁻¹) in soil according to the Mexican Regulation (DOF, 2005). This difference in values could be an important reason for the big difference in bioassay responses (both lethal and sublethal) among the different zones, as will be described below.

In the case of the lethal test with soybean (*Glycine max*), the highest lethality (42%) was obtained in Z2, with significant differences ($p < 0.05$) as compared to control. Samples that showed the lowest germination (50%) came from Z2 as well. The Z2 was the most toxic due to the high TPH levels (LC₅₀ = 17.8 mg kg⁻¹), followed by Z4 and Z1 (Table 2). The toxicological gradient was as follows: Z2 > Z4 > Z1 > Z3.

TABLE II INHIBITION OF GERMINATION (%) AND LC₅₀ FOR *G. MAX* AND *T. AESTIVUM*

Zone	Maximal inhibition of <i>G. max</i> germination (%)	Maximal inhibition of <i>T. aestivum</i> germination (%)	LC ₅₀ for <i>G. max</i> (mg kg ⁻¹ TPH)	LC ₅₀ for <i>T. aestivum</i> (mg kg ⁻¹ TPH)
Z1	39	31	518.3*	44.51
Z2	77*	63*	17.8*	3.56
Z3	38	30	NE	2072.12*
Z4	36	62	66.5*	7.48
Control	3	5	NA	NA

NE = No biological effect was observed in samples from Z3.

*Significant difference ($p < 0.005$). NA = Not applicable.

T. aestivum germination showed a similar pattern to that of *G. max* (Table 2). The highest toxicity was registered in Z2 with an LC₅₀ = 3.56 mg kg⁻¹ TPH. The gradient of toxic potential was also consistent with the results obtained with soybean. Results of *T. aestivum* germination using the dilution of soil extracts 0, 3.125, (6.25, 12.5, 25, 50, and 100%) showed the same significant difference ($p < 0.001$) between the control and the samples from zones. A dose-response curve using the above dilutions was performed, from which the inhibition of germination was obtained. Table 2 shows the maximal inhibition of germination and LC₅₀ for both plants.

In addition to the germination test, stem and root length (Table 3) was registered as an indirect measurement of the plant growth (Gomot-De Vaufleury, 2000). Considering this growth, there was significant difference ($p < 0.05$) between control and Z1 and significant difference ($p = 0.0017$) among control, Z2, and Z4.

TABLE III STEM AND ROOT LENGTH IN ADDITION TO PLANT BIOMASS FOR *G. MAX* AND *T. AESTIVUM*

Zone	Stem length (cm) for <i>G. max</i>	Stem length (cm) for <i>T. aestivum</i>	Root length (cm) for <i>G. max</i>	Root length (cm) for <i>T. aestivum</i>	Biomass <i>G. max</i>	Biomass <i>T. aestivum</i>
Z1	6.1	9.7	2.6	16.5	0.36	0.09
Z2	6.2	7.8	4.1	2.6	0.43	0.04
Z3	5.0	6.7	5.4	11.8	0.74	0.09
Z4	8.5	6.8	3.9	12.5	0.58	0.08
Control	16.4	12.7	6.5	16.6	1.05	0.12

An important aspect to deal with when assessing different toxicant's answers is the different sensitivity associated with the type of toxicant, which implies also different mechanisms of toxicity. Such is the case of germination inhibition by both TPH and PAH, their phytotoxicity is frequently associated with a blockade of seed imbibitions, referred as narcosis, which causes a lack of root emergency in the seed (Besaltpour et al., 2008). However, both root length and stem growth have more to do with PAH than with TPH, possibly due to endocrine disruption caused by these aromatic compounds.

Results obtained at the first level of response (lethal) using *Eisenia foetida* showed statistical differences among zones ($p < 0.05$). At the second level of response (sublethal), Z2 showed an elevated mortality (83%), whereas in Z1, 50% of the organisms died. In the rest of the organisms, only a decrease in mobility was observed. In Z3 and Z4, the highest mortality of *E. foetida* (40%) occurred during the bioassay using the soil extract from Z3. In Z4, 10% mortality was measured. Using the dose-response curve to obtain LC₅₀ for *E. foetida*, the highest toxicity was observed in Z2, with an LC₅₀ = 310 mg kg⁻¹ TPH. The toxicological gradient was as follows: Z2 > Z1 > Z3 > Z4. In Z2, the EC₁ = 0.047 mg kg⁻¹ and 0.17 mg kg⁻¹ in Z4.

The toxicity values obtained with Microtox® were the highest in Z4, followed by Z2 and Z1. Toxic Units (TU = 100/EC₅₀) exceed the Microtox scale for toxicity (over 4500 TU; Eom et al., 2007) for Z4 (Figure 2).

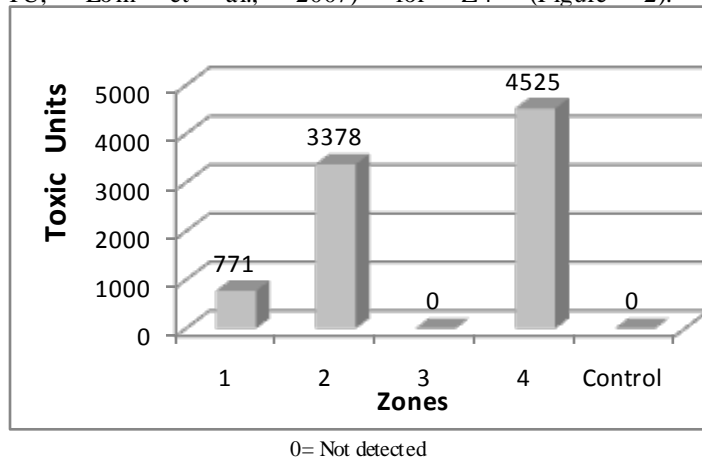


Figure 2 Mean Toxic units at 15 min obtained with Microtox®

Using the results from the sublethal response, the threshold level was calculated. This level, which is equivalent to EC₁, represents the lowest dose of a chemical at which a specified measurable effect for wetland biota is observed and, below it, no effect can be observed.

Sublethal results of plant length and biomass of *G. max* and *Triticum aestivum* using soil extract and Microtox® results suggest consistently that Z4 is the zone with the greatest relation in the dose-response curve (Table 4).

TABLE IV TPH EFFECTIVE CONCENTRATION (MG KG⁻¹) FOR PLANTS AND MICROTOX®

Zone	Equation	EC ₁	EC ₅₀
<i>Glycine max</i>			
Z4-SL	y = -1.8229x + 16.755, r = 0.94	12600.2	15901.5
Z4-RL	y = -0.4869x + 7.1526, r = 0.88	5450.3	10359.2
Z4-B	y = -0.0761x + 0.9897, r = 0.69	843.9	5922.2
<i>Triticum aestivum</i>			
Z2-SL	y = -1.496x + 15.029, r = 0.78	33515.4	42759.0
Z2-RL	y = -1.755x + 20.482, r = 0.64	45623.1	55628.2
Z2-B	y = -0.0122x + 0.177, r = 0.60	2.6	11370.9
Microtox®			
Z2	Logy = 0.8583xLog + 1.526, r = 0.93	1.6	3.0
Z4	Logy = 0.7239xLog + 2.183, r = 0.73	2.1	126.6

SL = Stem length, RL = Root length, B = Biomass.

When performing the MANOVA test (Table 5) using as dependent variables the LC₅₀, EC₅₀ and EC₁, and as variation factors the study areas and toxicity bioassays, we observed the following gradient of toxicity for the studied areas: Z2 > Z4 > Z3 > Z1 > ZC, being the control zone the least toxic (F_{4, 20} = 20.1, p < 0.001). This battery of tests and evaluated responses confirmed Z2 with the highest toxic potential in terms of both PAH and TPH and for both lethal (LC₅₀ F_{4, 40} = 2.7, p = 0.01) and sublethal responses (EC₁ = 16.89 with F_{4,40}, p = 0.004).

TABLE V MANOVA RESULTS

Source	Dependent Variable	df	Mean Square	F	Significance
Model	LC ₅₀ ^a	8	2027.892	2.827	.017
	EC ₁ root ^b	8	398901870.301	4.988	.000
	EC ₁ biomass ^c	8	1790938177.457	11.802	.000
	EC ₁ stem ^d	8	425806569.171	20.195	.000
Zone	LC ₅₀	4	1936.769	2.700	.048
	EC ₁ root	4	192438345.532	2.406	.070
	EC ₁ biomass	4	719808552.139	4.744	.004
	EC ₁ stem	4	356156540.974	16.892	.000
Bioassay	LC ₅₀	3	985.777	1.374	.268
	EC ₁ root	3	572695666.268	7.161	.001
	EC ₁ biomass	3	1596897022.264	10.524	.000
	EC ₁ stem	3	187060331.287	8.872	.000
Error	LC ₅₀	32	717.221		
	EC ₁ root	32	79969080.559		
	EC ₁ biomass	32	151742550.271		
	EC ₁ stem	32	21084363.062		
Total	LC ₅₀	40			
	EC ₁ root	40			
	EC ₁ biomass	40			
	EC ₁ stem	40			

^a r² = 0.41 (adjusted r² = 0.26), ^b r² = 0.55 (adjusted r² = 0.44), ^c r² = 0.74 (adjusted r² = 0.68), ^d r² = 0.83 (adjusted r² = 0.79)

Regarding the sensitivity of the bioassay, Microtox® test is more sensitive, followed by *E. foetida*, *G. max*, and finally the least sensitive was *T. aestivum* (p < 0.001).

Bioassays using organisms with different ecologic niche by biologic group have proven to be efficient tools for the detection of acute and subchronic toxicity and bioavailability, although they do not evaluate the medium and long term effects. However, in this case, bioassays with different exposure ways were used to determine toxicity potential because they all have different sensitivity to soil toxicity. The difference in sensitivity to hydrocarbons (TPH and PAH) is determined mainly by two factors, firstly the type of pollutant and the type of organism, based on bioconcentration, biotransformation, and the extent of damage, and secondly the ability to recover from it.

Thus, the toxicity levels would be a function of the soil composition of wetland, because all these organisms have a close interaction with the soil as substrate for their lifestyle. *V. fisheri* due to the direct exchange of gases and materials through the bacterial cell membrane, *E. foetida* through the soft skin of the digestive tract, and stem and root length of *G. max* and *T. aestivum* (Hubalék et al., 2007).

Using the results from the MANOVA analysis, and taking into account all of the bioassays and their endpoints, together with the hydrocarbon chemical analyses, we arrived at decisions regarding the toxicity potential depending on ecologic niche by biologic group.

Despite high sensitivity, results for microbial trophic level (Microtox®) and primary consumers (*E. foetida*) were not significant (p < 0.05) to determine toxicity potential. However, for primary producers level, there were significant differences, therefore considering the bioassays with wheat (*T. aestivum*), with higher sensitive, the level of toxic potential was 3,081.68 mg kg⁻¹ TPH (p = 0.013), whereas in the case of soybean (*G. max*), the determined value was 1,376.58 mg kg⁻¹ TPH (p < 0.001).

From the 16 EPA priority PAH analyzed, B(a)P was the only that exceeded the maximum permissible limit according to the Mexican Regulation. Based on the importance of plants as primary producers, they were selected to conduct the assessment of soil (sublethal concentrations), as done by some authors (e.g., Baird et al., 2007; Wilkea et al., 2008). We performed interpolation of the EC₁ to use this concentration as endpoint of lower toxicity response and therefore of higher sensible response. Results are shown in Table 6.

TABLE VI BENZO(A)PYRENE EFFECTIVE CONCENTRATION (MG KG⁻¹) FOR *G. MAX*

AND *T. AESTIVUM*

	<i>Glycine max</i> Zone 4		<i>Triticum aestivum</i> Zone 2	
	EC ₁	EC ₅₀	EC ₁	EC ₅₀
Stem	4.9092	12.9615	0.1029	6.3382
Root	1.1945	2.8898	0.3366	2.2587
Biomass		51.9643		21.2678

According to the results of root length with soybean using B(a)P (Table 6), the greatest toxic potential was found in Z4

with an $EC_{50} = 2.8898 \text{ mg kg}^{-1}$, whereas that for wheat was found in Z2 with an $EC_{50} = 2.2587 \text{ mg kg}^{-1}$, being wheat the most sensitive species. The B(a)P threshold value for soybean using root length was $EC_1 = 1.19 \text{ mg kg}^{-1}$ whereas for wheat it was $EC_1 = 0.34 \text{ mg kg}^{-1}$. The minimal sensitive level obtained (0.34 mg kg^{-1}) is much lower than 3 mg kg^{-1} (ATSDR, 2010; Bradley et al., 1994), and 2 mg kg^{-1} as established in Mexico for agriculture use (DOF, 2005).

IV. CONCLUSIONS

Currently, only a few soil guidelines for TPH are available to protect terrestrially ecological receptors (US EPA, 1997). An absence of basic ecotoxicological datum restrains the development of ecological soil screening values for TPH (Wang, 2010). Therefore the use of bioassays is recommended for ecotoxicological evaluations to determine sensitive between bioassays and toxicity gradient between zones.

In addition to the hydrocarbon concentration levels, the ecologically relevant criteria for estimating the impacts of petroleum hydrocarbons are also important end points for risk assessment, which contributes to protect the biodiversity of the ecosystem.

ACKNOWLEDGEMENTS

Financial and material support for this study was provided by PEMEX and Instituto Mexicano del Petróleo. R. Uribe-Hernández and M. A. Amezcua-Allieri are grateful for SNI fellowship.

REFERENCES

- Anzur (1998) "Microtox® Acute Toxicity Test Manual" Newark, Delaware, USA, 135 pp.
- ATSDR (2010) "Public Health Assessments and Health Consultations" Agency for Toxic Substances and Disease Registry, Atlanta, Georgia, USA, 195 pp.
- Baird, D., Van den Brink P. (2007). Using biological traits to predict species sensitivity to toxic substances. *Ecotox Environ Safety* Vol.67, pp. 296-301.
- Besalpour, A., Hajabbasi, MA., Afyuni, M. (2008). Germination and growth of selected plants in a petroleum contaminated calcareous soil. *Soil Sediment Contam* Vol.17, pp. 665-676.
- Bradley, L.J.N., Magee, B.H., Allen, S.L. (1994). Background levels of polycyclic aromatic hydrocarbons and selected metals in New England urban soils. *J Soil Contam* Vol.3, pp.1-13.
- DOF (Diario Oficial de la Federación) (2005) "NOM-138-SEMARNAT/SS-2003, Límites máximos permisibles de hidrocarburos en suelos y las especificaciones para su caracterización y remediación" México, 25 pp.
- ECOR (2002) "Restoration criteria in Ontario's land-use guideline" Environmental Protection Branch Environmental Contaminants and Nuclear Programs Division. ECOR, Ontario, Canada, 125 pp.
- Eisentraeger, A., Hund-Rinke, K., Roemtko, J. (2005). *Soil Biology*, Volume 5.
- Handbook for Soil Analysis. R. Margesin, F. Schinner. Eds. Springer-Verlag, Berlin, Germany. pp1-13.
- Eom, I.C., Rast, C., Veber, A.M., Vasseur, P. (2007). Ecotoxicity of a polycyclic aromatic hydrocarbon (PAH)-contaminated soil. *Ecotoxicology and Environmental Safety* Vol. 67, pp.190-205.
- Finney, D.J. (1978) "Statistical method in biological assay" Charles Griffin, London. pp. 89.
- Gomot-De Vaufléury, A. (2000). Standardized growth toxicity testing (Cu, Zn, Pb, and Pentachlorophenol) with *Helix aspersa*. *Ecotoxicology and Environmental Safety* Vol. 46, pp.41-50.
- Hubalék, T., Vosahlova, S., Mateju, V., Kovacova, N., Novotny, C. (2007). Ecotoxicity monitoring of hydrocarbon-contaminated soil during bioremediation: a case study. *Arch Environ Contam Toxicol* Vol. 52, pp. 1-7.
- ISO (2003a) "ISO 11268 Soil Quality- Effects of Pollutants on Earthworms (*Eisenia foetida*)" Part 1. Method for the Determination of the Acute Toxicity Using Artificial Soil Substrate. USA. pp. 37.
- ISO (2003b) "ISO 11269: Soil Quality- Determination of the Effects of Pollutants on Soil Flora" Part 2 Effects of Chemicals on the Emergence and Growth of Higher Plants, USA. pp. 67.
- Iturbe, R., Flores, R., Flores, C., Torres, L. (2004). TPH-contaminated Mexican refinery soil: health risk assessment and the first year of changes. *Environ Monit Assess* Vol. 91, pp. 237-255.
- Kmet, P. (2001) "Calculations for Table 740-1. Method A Soil Cleanup Levels for Unrestricted Land Uses" Department of Ecology, Washington, USA. pp. 175.
- OECD (1984) "Guideline 208 Terrestrial plants, growth test. OECD Guidelines for testing of chemicals OECD" Paris, France, pp. 17.
- Riser-Roberts, E. (1998) "Remediation of Petroleum Contaminated Soils. Biological, Physical and Chemical Processes". CRC Press, Boca Raton, Florida, USA. pp. 153.
- Salisbury, F.B., Ross C.W. (1985) "Plant Physiology". Wadsworth, California, USA, pp. 127.
- Uribe-Hernández, R., Montes de Oca-García, M.A., Zermefio-Eguía, Lis. J.A., Salazar-Coria, L., Martínez-Martínez, V.E. (2004). Ecotoxicity assessment of phytoremediation treatment of oil spills on fresh marsh in the Mexican southeast, Proceedings of Seventh International in situ and on site Bioremediation Symposium, Battelle Memorial Institute, Orlando, Florida, USA, pp. 15.
- US EPA (1996) "Seed germination/root elongation toxicity test. Ecological effects test guidelines USEPA-OPPT S850.4200. [WWW document] <http://www.epa.gov/OWOW/wetlands/wqual/ppindex.html>.
- US EPA (1997) "Ecological risk assessment guidance for superfund: Process for designing and conducting ecological risk assessments (interim final)". US EPA/540/R-97/006. [WWW document] <http://www.epa.gov/OWOW/wetlands/wqual/ppindex.html>.
- US EPA (1998) "Test methods for evaluating solid waste, physical/chemical methods. EPA publication SW-846. [WWW document] <http://www.epa.gov/OWOW/wetlands/wqual/ppindex.html>.
- US EPA (2000) "Method 3550C. Ultrasonic extraction" Environmental Protection Agency, Washington, USA, pp. 48.
- US EPA (2006) "National wetlands status and trends study and report" U.S. Fish and Wildlife Service. [WWW document] <http://www.epa.gov/OWOW/wetlands/wqual/ppindex.html>.
- Shi-Jie, W., Zeng-Guang, Y., Guan-Lin, G., Gui-Lan, L., Qun-Hui, W., Fa-Sheng, L. (2010) Ecotoxicity assessment of aged petroleum sludge using a suite of effects-based end points in earthworm *Eisenia fetida*. *Environ Monit Assess* Vol. 169, pp. 417-428.
- Wilkea, B.M., Riepert, F., Kocha, C., Kuhne, T. (2008). Ecotoxicological characterization of hazardous wastes. *Ecotox Environ Safety* Vol. 70, pp. 283-293.

Raúl Uribe-Hernández he received a B.Sc. (1990) in Biology from the National Autonomous University of Mexico (UNAM), a M.Sc. (1995) in Toxicology and a Ph. D. (2006) in Chemical-Biologic Sciences from National Polytechnic Institute (IPN). Currently, he works for the Mexican Petroleum Institute as an expert and leader of environmental and health risk assessment service. He is professor of Toxicology *in vitro* in the Life Sciences School at IPN.

Marco Alejandro Montes de Oca-García received his B. Sc. (1983) in Biochemical Engineering from IPN and a M. Sc. (1991) from the Universidad Autónoma Metropolitana-Mexico. He holds a specialization in petroleum microbiology (1989) from the JICA - Japan at the Fermentation Research Institute. He works for the Mexican Petroleum Institute in characterization, monitoring and remediation of contaminated soils as a Technical Consultant.

Myriam Adela Amezcua-Allieri holds a B. Sc. in Biology (honours) from UNAM, a Master in Science degree (Environmental Engineering) from IPN and a Ph. D. (honours) in Geography and Environmental Sciences from The University of Birmingham, UK. Areas of interest: bioremediation of soil contaminated with hydrocarbons and metals, contaminant bioavailability and speciation, impact of petroleum industry in environment. In 2010 she received the Award for Young Women Scientists in Biology for the Latin America and Caribbean Region sponsored by Elsevier Foundation and the Third World Organization for Women in Science (TOWS).

Juan Antonio Zermeño-Eguía Lis received a B. Sc. (1983) as Chemist, Bacteriologist and Parasitologist (QBP) from IPN and a M. Sc. (2001) in Chemical Biologic Sciences from IPN in Mexico City. He works for the Mexican Petroleum Institute in management of hazard waste and remediation of contaminated soils with hydrocarbons in environmental projects.

Víctor Emigdio Martínez-Martínez received his B. Sc. (1986) in Agricultural Engineering from UNAM and a M. Sc. (2000) in Environmental Engineering from IPN. Currently he is the leader of Soil Remediation Service, at the Mexican Petroleum Institute.